Satellite Products and Services Review Board

Algorithm Theoretical Basis Document

NOAA Blended VIIRS/ABI Flood Mapping (BFM) Product

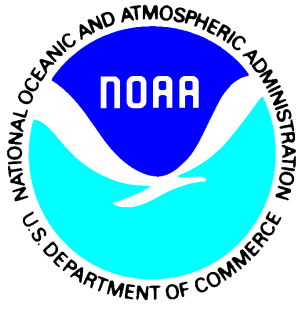

Version 1.1

May 2024

TITLE: Blended VIIRS/ABI Flood Mapping (BFM) Algorithm Theoretical Basis Document

AUTHORS:

Sanmei Li, George Mason University

Sean, Helfrich, NOAA/STAR

Donglian Sun, George Mason University

DOCUMENT HISTORY
DOCUMENT REVISION LOG

Blended VIIRS/ABI Flood Mapping (FM) Algorithm Theoretical Basis Document			
DOCUMENT CHANGE HISTORY			
Revision No.	**Date**	**Revision Originator Project Group**	**CCR Approval # and Date**
1.0	May 2024	No version 1.0	N/A
2.0	July 2024	No version 1.1	
2.1			
2.2			

LIST OF CHANGES

Significant alterations made to this document are annotated in the List of Changes table.

Blended VIIRS/ABI Flood Mapping (FM) Algorithm Theoretical Basis Document					
LIST OF CHANGE-AFFECTED PAGES/SECTIONS/APPENDICES					
Version Number	**Date**	**Changed By**	**Page**	**Section**	**Description of Change(s)**

Table of Contents

LIST OF TABLES AND FIGURES

1 INTRODUCTION

With the support from the JPSS (Joint Polar Satellite System) Proving Ground and Risk Reduction (PGRR) Program, the global 375-m flood products in near real-time, daily composition, and 5-day composition have been developed to derive flood extent represented in water fractions from VIIRS (Visible Infrared Imaging Radiometer Suite) imagery on-boarding Suomi-NPP, NOAA-20 and NOAA-21. Although VIIRS imagery provide excellent data sources for flood mapping, the polar-orbit satellites only have one to two observations in mid-to-low latitudes, and thus they can be easily affected by cloud and cloud shadows, resulting in latency and discontinuity on flood detection.

Later, under the support from GOES-R program, the ABI (Advanced Baseline Imager) imagery, which are available every 5 minutes in the CONUS and every 10 minutes in the full disk and provide flood detection with timely manner that no other satellites can reach, have been integrated in the flood mapping software to generate ABI 1-km flood products from GOES-16&17&18&19. The ABI flood maps successfully capture the maximal clear-sky coverage during daytime. However, the 1-km coarse resolution near nadir is a limit for the ABI flood products to show inundation detail, especially in mid-to-high latitudes.

Considering VIIRS and ABI flood products have their own advantages in flood mapping, if the two products can be merged together, then a new blended VIIRS/ABI flood product could be derived, which has VIIRS's fine resolution and ABI's maximal clear-sky coverage and thus shows the best result for flood mapping.

This Algorithm Theoretical Basis Document (ATBD) describes in detail the procedures for developing blended VIIRS/ABI flood mapping algorithms. It includes a description of the requirements and specifications of the blended VIIRS/ABI flood product and some specific information that is relevant to the derivation of the blended product. The main part of the ATBD is a description of the science of the blended VIIRS/ABI flood-mapping algorithm, followed by the assumptions and limitations of the algorithm and products in flood mapping.

1.1 Product Overview

1.1.1 Product Description

The blended VIIRS/ABI flood product, referred as BFM (blended flood mapping), is a level-3 flood product based on the level-2 VIIRS and ABI flood products. The product is to fuse the two flood products with different spatial resolution into one product at a fine resolution. The Algorithm Theoretical Basis Document for VFM and AFM is referred in the document (link: https://www.star.nesdis.noaa.gov/jpss/documents/ATBD/ATBD_VIIRS_Flood_Mapping_v1.0.pdf). The BFM is a new product, which means there are no existing operational algorithms or products to inherit from the previous satellite missions or programs.

The blended VIIRS/ABI flood products include a blended VIIRS/ABI flood product using a nearest neighboring interpolation method and a blended VIIRS/ABI flood product using a simplified downscaling method. Both the two products are with the same spatial coverage to AFM. Table 1-1 lists the two products produced in the operational system.

Table 1-1 Blended VIIRS/ABI flood products produced in the operational system

Product name	Spatial resolution	Geographic Coverage	Temporal Coverage	Description
Blended VIIRS/ABI flood product using nearest neighboring interpolation method	375 m	American mainland and islands between 50.5°S and 50.5°N	Daily	VIIRS and ABI flood products are merged using nearest neighboring interpolation method
Blended VIIRS/ABI flood product using simplified downscaling method	375 m	American mainland and islands between 50.5°S and 50.5°N		VIIRS and ABI flood products are merged using a simplified downscaling method

1.1.2 Product Requirements

The requirements of blended VIIRS/ABI flood products are listed in Table 1-2.

Table 1-2 Requirements of blended VIIRS/ABI flood products

Product name	Formats	Latency	Measurement range	Product accuracy
Blended VIIRS/ABI flood product using nearest neighboring interpolation method	netCDF4	1 hours after daily VIIRS and ABI composites become available	Water fraction≥25%	80% under clear-sky conditions
Blended VIIRS/ABI flood product using simplified downscaling method	netCDF4, geotiff and shapefile	1 hours after daily VIIRS and ABI composites become available	Water fraction≥25%	80% under clear-sky conditions

2 ALGORITHM DESCRIPTION

A comprehensive description of the blended VIIRS/ABI flood mapping algorithm and data flow is presented in this section.

2.1 Processing Outline

The major procedures of the blended VIIRS/ABI flood mapping system include blending process in two different methods: nearest neighboring interpolation method and a simplified downscaling method, and image display. Fig. 2-1 shows the system architecture and data flow. In Fig. 2-1, the VIIRS and ABI daily composited datasets are ingested in the system and then applied with the nearest neighboring interpolation method and the simplified downscaling method, respectively to derive blended flood maps. The image display module converts the blended results in netCDF4 outputs to raster images in geotiff and png formats and vector data in shapefile format.

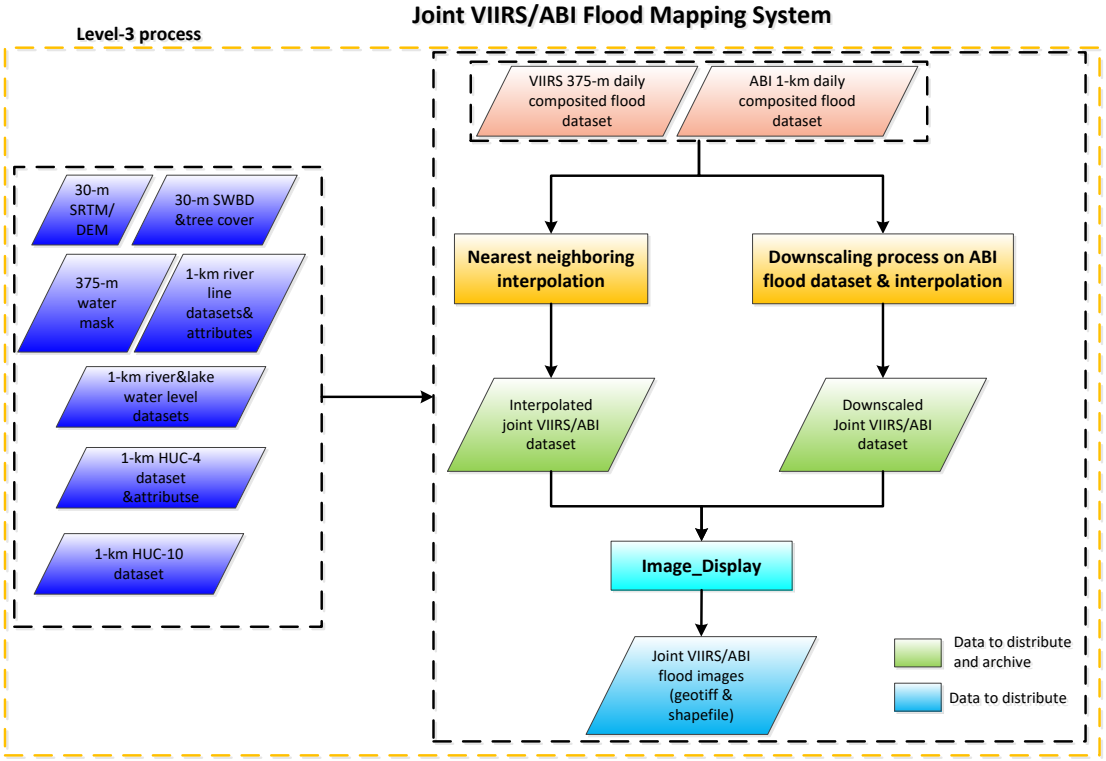

Fig. 2-1 Flowchart of the blended VIIRS/ABI flood mapping system

Blending with the nearest neighboring interpolation method is a very simple and straightforward process. It takes the VIIRS results as the base map, and uses the clear-sky detection results from ABI flood maps to fill the gaps of clouds and cloud shadows in the VIIRS flood maps through nearest neighboring interpolation. The method does not really change the resolution of ABI flood detection results, but just simply overlaps the ABI results on VIIRS flood maps.

In comparison, the simplified downscaling method is more complex. Similarly, it uses the VIIRS flood maps as the base maps, and the cloud and cloud shadow pixels are replaced either with ABI results directly if they are non-flooded clear-sky pixels in the ABI flood maps, and/or with ABI flood pixels through a downscaling-upscaling process if they are flood pixels in ABI results. The downscaling-upscaling process is a process that downscales the ABI 1-km floodwater fractions into 30-m flood extent with high-resolution DEM data and then up-scales the 30-m flood extent into 375-m floodwater fractions.

Fig. 2-2 presents the process flow of the blended VIIRS/ABI flood mapping algorithm. Details of the algorithm are demonstrated in section 2.3.

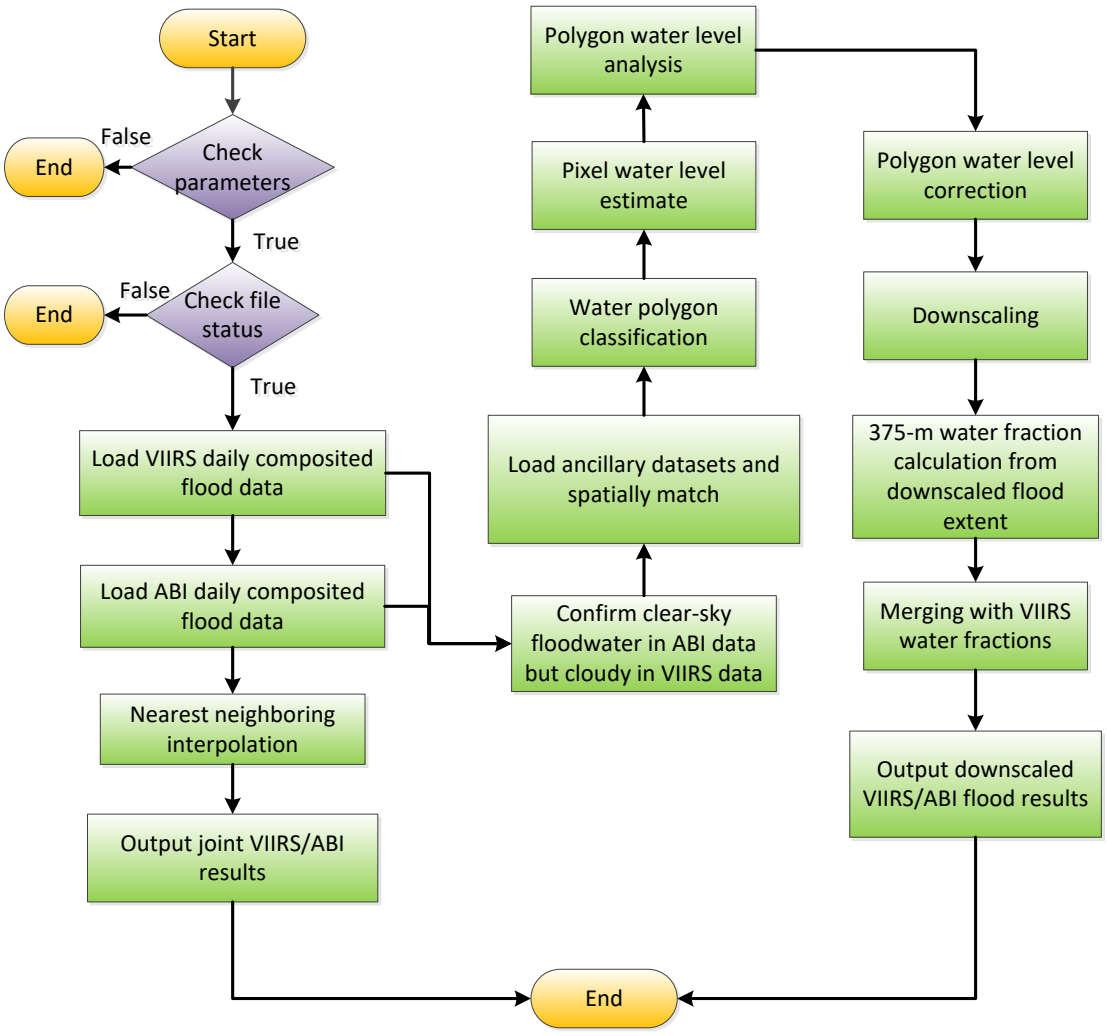

Fig. 2-2 Flow chart of the blended VIIRS/ABI flood mapping algorithm

2.2 Algorithm Input

The input data of the blended VIIRS/ABI flood detection algorithm include:

- VIIRS daily composited flood detection dataset;
- ABI daily composited flood detection dataset;
- Static ancillary datasets: 30-m Copernicus Digital Surface Model (CDSM) data, 30-m merged SWBD and MLCD data (water mask and tree cover), 375-m water mask, 1-km river line data, 1-km river/lake water level data, 1-km HUC level-8 data and HUC level-10 data.

Table 2-1 lists all the input datasets used in BFM.

Table 2-1 Specifications of BFM input data

Input File	Spatial Resolution	Name Pattern	Content	Format
VIIRS daily composites	375m	e.g. VIIRS-Flood-1day-GLB023_v1r0_blend_s201708311838380_e201708312025190_c202206170717217.nc	VIIRS daily composited flood detection results	netCDF
ABI daily composites	375m	e.g. ABI-Flood-DCOM-AOI003_v1r0_g16_s201708311500343_e201708312256108_c202307252105028.nc	ABI daily composited flood detection results	netCDF
30-m CDSM data	30m	e.g. Copernicus_DSM_COG_10_N40_00_W096_00_DEM_30m.raw	Copernicus Digital Surface Model	raw
30-m water mask and tree cover data	30m	e.g. swbd_treecover2010_40N_090W_25m.raw	Merged SWBD and MLCD data	raw
1-km river line data	1 km	e.g. ABI_1km_Hydro_River_na_ca_sa_10314_11564.raw	River lines	raw
1-km river/lake water level data	1 km	e.g. ABI_1km_Hydro_riverlake_waterlevel_na_ca_sa_10314_11564_CDSM.raw	River/lake water levels	raw
1-km HUC level-08 data	1 km	e.g. ABI_1km_Hydro_HUC04_na_ca_sa_10314_11564.raw	Hydrologic Unit Code Level-08 data	raw
1-km HUC level-10 data	1 km	e.g. ABI_1km_Hydro_HUC10_na_ca_sa_10314_11564.raw	Hydrologic Unit Code Level-10 data	raw

2.3 Theoretical Description

2.3.1 Physical Description

The nearest neighboring interpolation method is a very simple method. The method firstly spatially matches the ABI flood maps with the VIIRS flood maps, and then takes the VIIRS flood maps as base maps, and any floodwater pixels in the VIIRS flood map are used as floodwater pixels in the blended flood maps. For cloud/cloud shadow pixels in the VIIRS flood maps, if they are with floodwater or clear-sky dry land in the ABI flood maps, then these pixels are assigned with ABI flooding water fractions or clear-sky dry land in the blended flood map.

The physical basis of the simplified downscaling process method is based on water's self-leveling nature. In natural topography, water always accumulates from lower levels to higher levels in elevations and flows from higher elevations to lower elevations connectively. Under certain topographic conditions with topography slopes between 0ºand 90º, certain relationship exists between water surface level and water area. This relationship can be used to estimate water surface levels from satellite-based areal flood extent. Because the retrieved floodwater fractions in the VIIRS and ABI flood maps indicate open water areas in VIIRS 375-m pixels or ABI 1-km pixels, they can be used to estimate water surface levels with high-resolution DEM data. The key to estimate water surface levels from VIIRS and ABI flood maps is to make VIIRS and ABI retrieved water areas equal to the corresponding water areas derived from DEM, which is called DEM-based water area, by iterating surface elevations from the lowest point to the highest point. With this conception, the inundation mechanism between VIIRS or ABI water area and DEM-based water area can be expressed in Equation (1):

$$A = \int_{min\_h}^{max\_h} f(h)dh \quad (1)$$

Here, A is the total water area or water fraction retrieved from VIIRS or ABI, $f(h)$ is the increment of water area between the minimal surface elevation min_h derived from DEM and maximal inundated surface elevation max_h.

The inundation mechanism expressed in Equation (1) is called a simplified downscaling mechanism because it ignores the impact from tree cover or urban constructions. A simplified downscaling method is applied for deriving blended VIIRS/ABI flood product because the final spatial resolution of the product is 375m instead of 30m, and uncertainties from tree cover and urban constructions may not change much on the quality of the results.

2.3.2 Mathematical Description

2.3.2.1 Description of nearest neighboring interpolation

The nearest neighboring interpolation method is applied to keep the original information from the VIIRS and ABI flood maps. This method does not change the resolution of ABI flood maps, but directly use the original ABI clear-sky detection results to fill the gap of cloud and cloud shadow in the VIIRS flood maps.

In the blended VIIR/ABI flood dataset, if a pixel is in clear-sky condition (dryland, snow/ice or floodwater) in the corresponding VIIRS daily composited flood map, then it is assigned with the clear-sky detection result from the VIIRS flood map. If a pixel is detected

as cloud or cloud shadow in the VIIRS flood map, but is in clear-sky condition in the ABI daily composited flood map, and then it is assigned with the clear-sky detection result from the ABI flood map. If it is also detected as cloud or cloud shadow in the ABI flood map, then it is assigned with cloud or cloud shadow in the blended dataset.

Fig. 2-3 presents a blended VIIRS/ABI flood map using nearest neighboring interpolation method on Aug. 18, 2018. In Fig. 2-3, because the spatial resolution of ABI floodwater is not changed, they show much coarser floodwater boundaries in the blended flood map than floodwater from VIIRS.

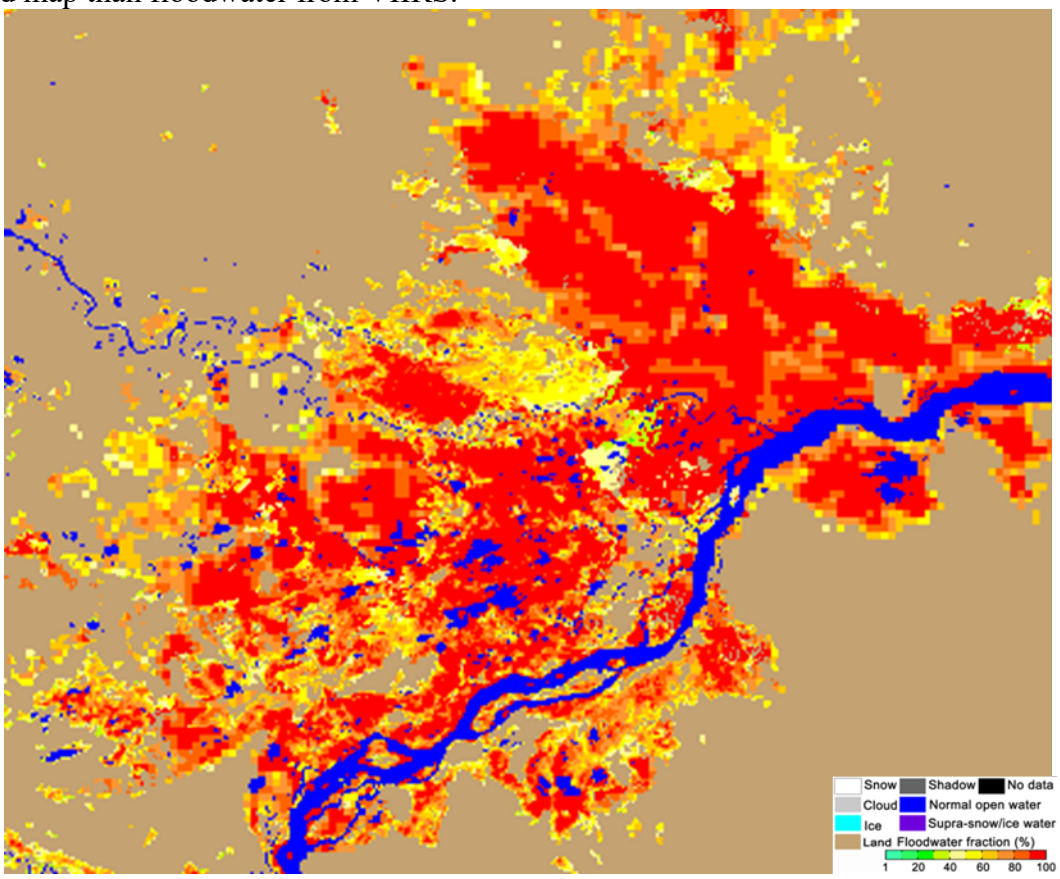

Fig. 2-3 An example of blended VIIRS/ABI flood map using nearest neighboring interpolation method on Aug. 18, 2018

2.3.2.2 Description of the simplified downscaling process

The simplified downscaling process is used to downscale the ABI 1-km floodwater fractions to 30-m flood extent by using 30-m CDSM data and other ancillary datasets. It includes pixel water level calculation, polygon water level estimate and downscaling.

2.3.2.2.1 Pixel Water Level Calculation

For each ABI floodwater pixel, water surface level can be coarsely estimated using Equation (1). First, the ABI flood maps are spatially matched with CDSM data. The ABI floodwater fractions can be used to compare with the total percentages of the inundated

cells in the CDSM. To derive DEM-based water percentage, the cell with the minimal surface elevation among all the cells corresponding to an ABI pixel is used as the starting cell to cluster the cells adjacent to each other by iterating surface elevation. Floods generally occur along rivers or lakes due to higher-than-normal river/lake levels, so starting cells are generally located over rivers or lakes. The SWBD dataset is used to help determine any existent river/lake cells within the ABI pixel. When the DEM-based water percentage is equal to ABI water fraction, the iteration is terminated and the final surface elevation is taken as the pixel water level.

2.3.2.2.2 Polygon Water Level Calculation

The pixel water level described in Section 2.3.2.2.1 is a rough estimate because of the uncertainties existing in the ABI water fraction retrieval and the coarse vertical resolution of CDSM. According to water's fluid features, in natural topography, if surface elevations are similar, water surface levels are similar. That means for neighboring water pixels, if they have similar surface elevations, their water levels should be similar. Based on this conception, neighboring water pixels with similar surface elevations can be clustered into a single water polygon and all the water pixels within this polygon should have the same water level. In this way, the uncertainties in the pixel water levels can be reduced.

To cluster neighboring water pixels with similar surface elevations into water polygons, river drainage, watershed and river distance datasets are used. Water pixels in the same watershed along a river are clustered into one water polygon, which is further divided into many small water polygons using river distance dataset. For a water polygon, water levels of all the floodwater pixels are used to determine the polygon water level. Water fraction difference at different water levels obtained from all the floodwater pixels in a water polygon are calculated, and the water level that causes the least water fraction difference is used as the polygon water level.

2.3.2.2.3 Downscaling with CDSM

With the derived polygon water levels, ABI flood maps can be downscaled into 30-m flood maps with the 30-m CDSM data. The downscaling process is done pixel-by-pixel. For an ABI 1-km floodwater pixel, the corresponding cells in the CDSM data are searched for a spatial match. The cell with the lowest surface elevation over river/lake surface is taken as the starting cell. A recursion method is applied using the N4(P) adjacency rule (only considering 2 horizontal and 2 vertical neighbors) to search the neighboring cells with surface elevations less than polygon water level (Li et al., 2013). The searched cells are assigned as floodwater cells.

Because most pixels with water fractions less than 30% are not detected in ABI flood maps, the derived 30-m flood extent from the downscaling process sometimes shows discontinuous floodwater distribution (Li et al., 2017). To avoid such situation, the downscaling process is also applied to the neighboring non-flood pixels using the same N4(P) adjacency rule. The surface elevations of the determined floodwater cells in the CDSM are used to compare with the cells adjacent to them. If cells within the neighboring non-floodwater pixels have lower elevations than the floodwater cells, they are determined as the floodwater cells.

In this way, the ABI 1-km flood maps can be downscaled into 30-m flood extent maps

2.3.2.3 Upscaling process

With the downscaled 30-m flood extent from ABI 1-km floodwater fractions, an upscaling process can be done to derive floodwater fractions at any spatial resolution coarser than 30m. For the blended VIIRS/ABI flood product, the chosen resolution is 375m to match with VIIRS's spatial resolution.

Similar to the nearest neighboring interpolation method, clear-sky pixels in the VIIRS flood maps are directly used in the blended VIIR/ABI flood dataset. For those cloud or cloud-shadow pixels in the VIIRS flood maps, if they are with floodwater pixels in the ABI flood maps, then these pixels are through a downscaling-upscaling process to derive 375-m floodwater fractions, and are then assigned to the blended VIIRS/ABI floodwater dataset.

Fig. 2-4 presents two blended VIIRS/ABI flood maps using nearest neighboring interpolation method (left) and using the simplified downscaling method on Aug. 30, 2017 in the West Gulf region of USA. In Fig. 2-4, the circled region shows a piece of floodwater from ABI flood map with different methods. In Fig. 2-4 (left), the circled floodwater is from nearest neighboring interpolation method, and In Fig. 2-4 (right), the circled floodwater is from the simplified downscaling method. Comparing to Fig. 2-4 (left), the circled water in Fig. 2-4 (right) is with much better resolution and clearer floodwater boundaries.

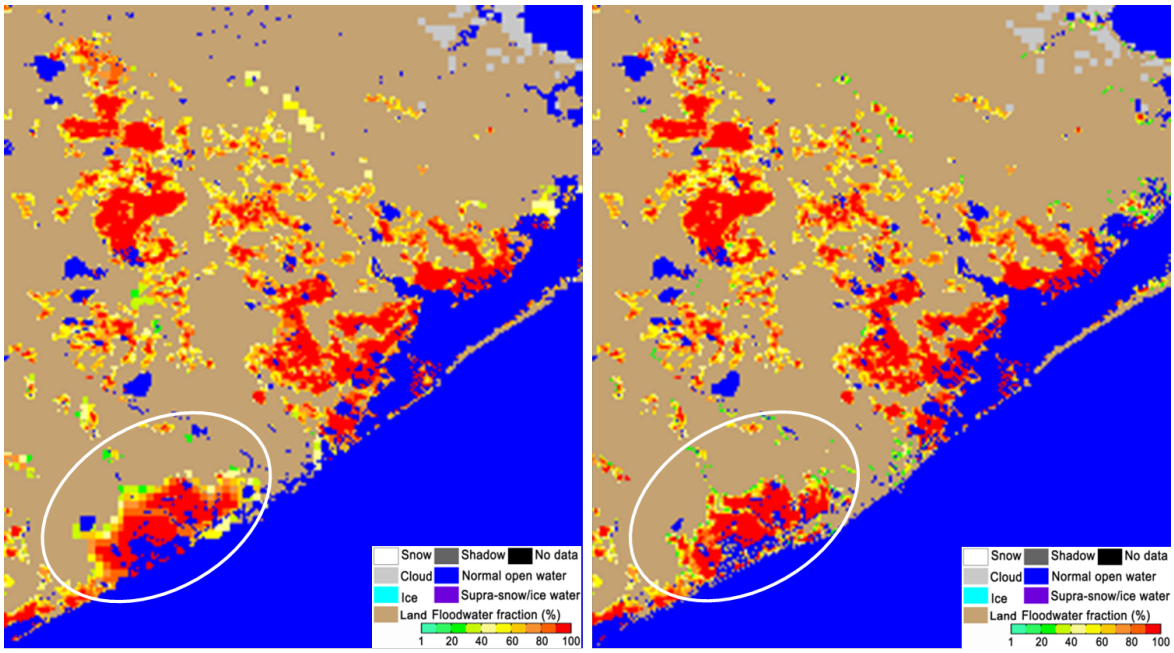

Fig. 2-4 Examples of blended VIIRS/ABI flood maps with different methods (left: from nearest neighboring interpolation method, right: from the simplified downscaling method)

2.4 Algorithm Output

The BFM algorithm outputs include:

- Blended VIIRS/ABI flood dataset using nearest neighboring interpolation method

- Blended VIIRS/ABI flood dataset using simplified downscaling process method
- Quality flag of the blended VIIRS/ABI flood dataset

The geographic coverage of the blended VIIRS/ABI flood product is the same with the ABI flood product (Fig. 2-5). The formats include netCDF, geotiff and shapefile. Ultimately, there are eight pixel types in the final blended VIIRS/ABI flood maps: cloud, snow cover, river/lake ice cover, shadows (including cloud shadows and terrain shadows), clear-sky land (including vegetation and bare soil), normal open water, supra-snow/ice water (including mixed water&ice and melting ice surface), and supra-veg/bare soil flooding water fractions. Data quality inherits the quality flags of the daily composites of VIIRS and ABI consequently. Table 2-2 lists the definition of the VIIRS output floodwater dataset, and the quality flags are shown in Table 2-3.

Table 2-2 Definition of types of WaterDetection dataset in the output BFM netCDF file

Value	Definition
1	Fill value: bad data, solar eclipse, data with solar zenith angles out of processing range
15	Open water without water fraction retrieval
16	Clear-sky bare land
17	Clear-sky vegetation
20	Snow cover
27	River/lake ice cover
30	Cloud cover
38	Supra-snow/ice water, mixed ice&water, or ice in melting status
50	Shadow: cloud shadow and terrain shadow
100	Open normal water: river, lake, reservoir, ocean
101~200	Water fractions of supra-vegetation bare land floodwater

Table 2-3 Definition of QualityFlag dataset in the output BFM netCDF file

Value	Definition
0	High-quality detection
1	Moderate-quality detection

2	Low-quality detection
255	Fillvalue

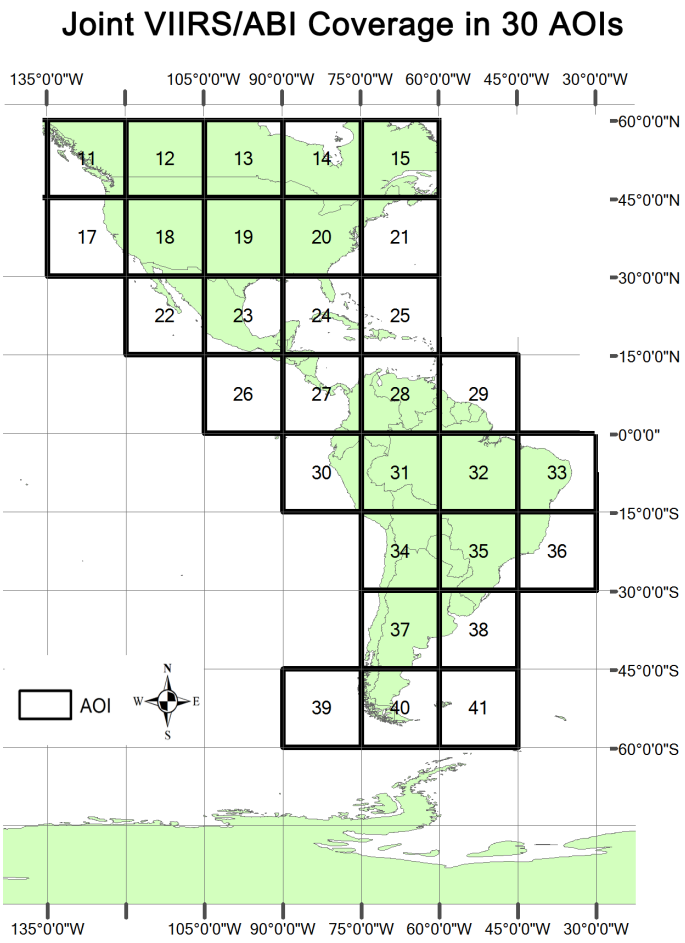

Fig. 2-5 Geographic coverage of blended VIIRS/ABI flood product

2.5 Performance Estimates

2.5.1 Test Data Description

One-day VIIRS and ABI daily composited datasets on Aug. 30, 2017 are chosen as the test data.

For VIIRS daily composites, there are altogether 30 AOIs covering the geographic range of the blended VIIRS/ABI flood product (Fig. 2-5).

For example, VIIRS daily composited data in AOI 23 on Aug. 30, 2017 is used as the VIIRS test data:

VIIRS-Flood-1day-GLB023_v1r0_blend_s201708301857340_e201708302044120_c202206170715445.nc

There are four domains of ABI daily composited product:

ABI-Flood-DCOM-AOI001_v1r0_g16_s201708301500360_e201708302256124_c202307252102023.nc

ABI-Flood-DCOM-AOI002_v1r0_g16_s201708301500360_e201708302256124_c202307252104003.nc

ABI-Flood-DCOM-AOI003_v1r0_g16_s201708301500360_e201708302256124_c202307252105010.nc

ABI-Flood-DCOM-AOI004_v1r0_g16_s201708301500360_e201708302226124_c202307252106004.nc

With the test data, lended_VIIRS_ABI_Flood_Version01 module ingests all the required data, and outputs the blended VIIRS/ABI flood file in netCDF format:

VIIRS-ABI-Flood-GLB023_v1r0_blend_s201708301857340_e201708302044120_c202307311920448.nc

With the Image_Display module developed in GDAL, the netCDF file is converted into geotiff, png and shapefile formats:

VIIRS-ABI-Flood-GLB023_v1r0_blend_s201708301857340_e201708302044120_c202307311920448.tif

VIIRS-ABI-Flood-GLB023_v1r0_blend_s201708301857340_e201708302044120_c202307311920448.png

VIIRS-ABI-Flood-GLB023_v1r0_blend_s201708301857340_e201708302044120_c202307311920448.shapefile.zip

More detail will be provided in “System Maintenance Manual”.

Fig. 2-6 shows result of the output file in AOI 23 on Aug. 30, 2017

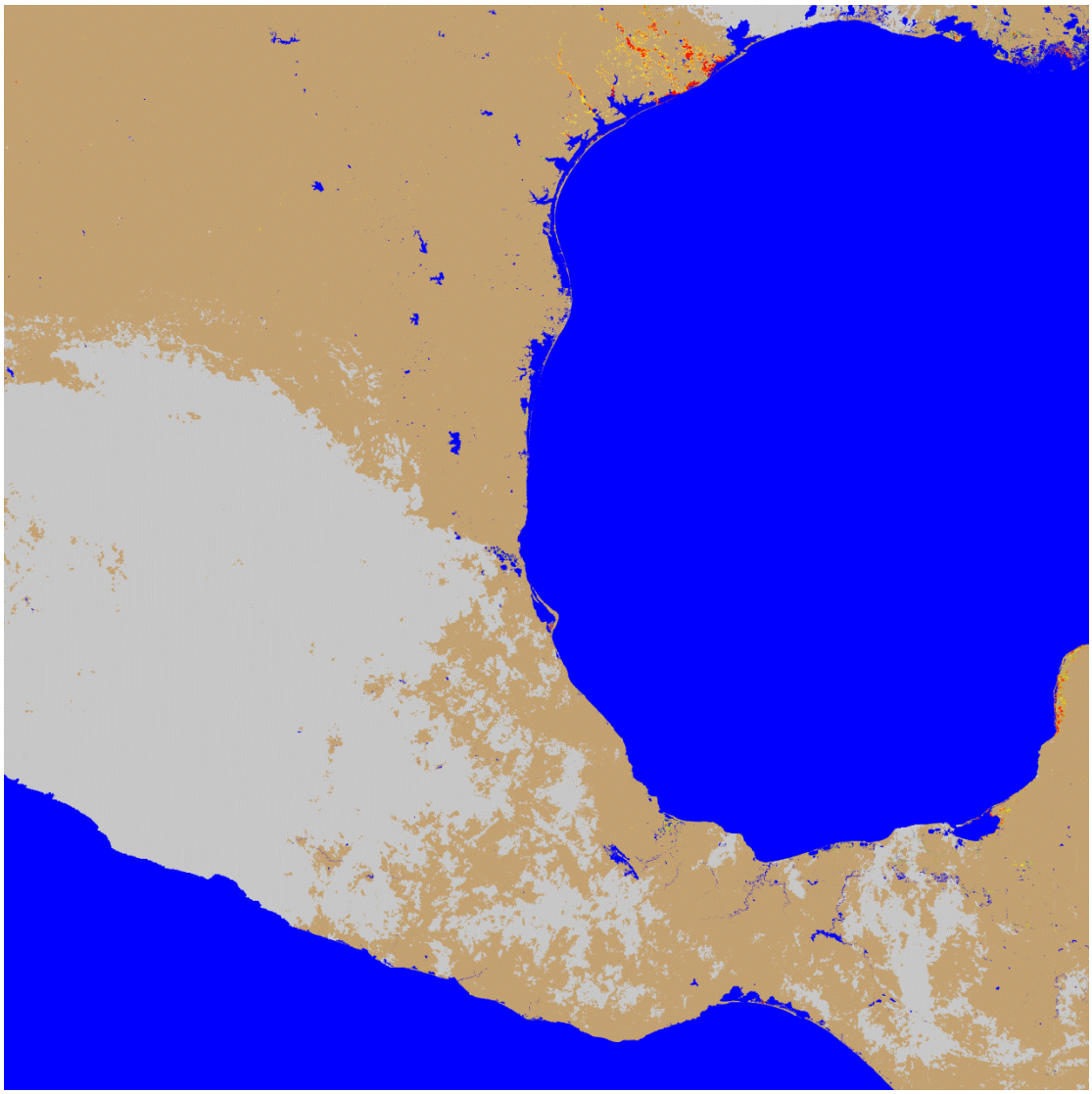

Fig. 2-6 Blended VIIRS/ABI flood map of the test result on Aug. 30, 2017 in AOI 23

2.5.2 Sensor Effects

The blended VIIRS/ABI flood product is a level-3 product based on VIIRS and ABI daily composited flood products. The sensor effects inherit from VIIRS and ABI daily composited flood products.

2.5.3 Retrieval Errors

The retrieval errors also inherit from VIIRS and ABI daily composited flood products.

The retrieval errors of the dataset using nearest neighboring interpolation are completely VIIRS and ABI daily composited flood products.

For the dataset using the simplified downscaling method, besides the inherited retrieval errors from VIIRS and ABI daily composited products, the downscaling process of the ABI floodwater fractions can cause uncertainties on the results, which are reflected in the following aspects:

Firstly, water polygon clustering may cause uncertainties by counting in some floodwater pixels that belong to other water polygons. Therefore, in one water polygon, some water pixels may get underestimated or overestimated water levels, resulting in inaccurate flood extent.

Secondly, polygon water levels are determined with the water level that causes the least water fraction difference. The uncertainties of ABI retrieved water fractions may cause uncertainties of polygon water levels.

Thirdly, the method is a simplified downscaling method to save computing resources, which ignores the impact from tree cover and urban constructions. The estimated water levels may not be accurate enough and then decrease the quality of the downscaled flood extent from ABI floodwater fractions.

Finally, the polygon water levels are not corrected through river network analysis and adjacent dryland flow test, which may cause uncertainties to the downscaled flood extent.

2.6 Practical Considerations

2.6.1 Numerical Computation Considerations

The downscaling process on ABI 1-km flood maps could take a long time if widespread flood occurs. To save computing resources, the BFM algorithm uses a simplified downscaling method, which could finish one AOI rapidly. Additionally, only those ABI floodwater pixels that are cloud or cloud shadows in the VIIRS flood maps are downscaled. The process on each AOI is independently, which means multiple jobs could be submitted simultaneously.

2.6.2 Programming and Procedural Considerations

The blended VIIRS/ABI flood product uses daily composited flood products from VIIRS and ABI. The process starts when the two products become available. Thus, it is generally available before next morning, which guarantees enough time for process.

2.6.3 Quality Assessment and Diagnostics

The quality flags of the blended VIIRS/ABI flood product completely inherit from VIIRS and ABI's quality flag datasets, depending on which dataset a pixel uses. Thus, the definition of the quality flags is the same with VFM and AFM products.

2.6.4 Exception Handling

There are altogether 32 error types defined to handle processing exceptions such as memory check, file access status check, file name check, file I-O success check and so on.

As long as VFM and AFM are available, the blended VIIRS/ABI flood product can be output unless there are errors from memory or disk failures.

2.7 Validation

Because VIIRS flood product is fully validated, validation on blended VIIRS/ABI flood product is done by comparing the downscaled ABI 375-m flood maps with VIIRS 375-m flood maps, as well as comparing with ABI 1-km flood maps to see whether the results have been improved.

Because VIIRS flood product does not show floodwater pixels with floodwater fractions less than 30%, floodwater pixels with water fractions less than 30% in the ABI downscaled 375-m flood maps and ABI 1-km flood maps are excluded. Thus, the comparison is done only on those floodwater pixels with floodwater fractions above 30%.

2.7.1 Visual inspection

The ABI downscaled 375-m flood maps are compared with ABI 1-km flood maps and VIIRS 375-m flood maps through visual inspection to confirm that the spatial distribution patterns are consistent to one and another.

Fig. 2-7 and Fig. 2-8 are two comparison examples. In Fig. 2-7, the ABI downscaled 375-m flood map (Fig. 2-7 left) shows consistent floodwater boundaries with VIIRS 375-m flood map (Fig. 2-7 right). Comparing to the original ABI 1-km flood map (Fig. 2-7 mid), most floodwater pixels with water fractions from 30% to 60% in the ABI 1-km flood map disappear in the ABI downscaled 375-m flood map due to the enhancement of spatial resolution. The distribution of floodwater fractions in the ABI downscaled 375-m flood map are much closer to that in the VIIRS 375-m flood map.

Fig. 2-8 presents similar results to Fig. 2-7. In Fig. 2-8, the ABI downscaled 375-m flood map (upper right) shows more consistent spatial distribution of floodwater fractions to VIIRS 375-m flood map (bottom right) than ABI 1-km flood map (left).

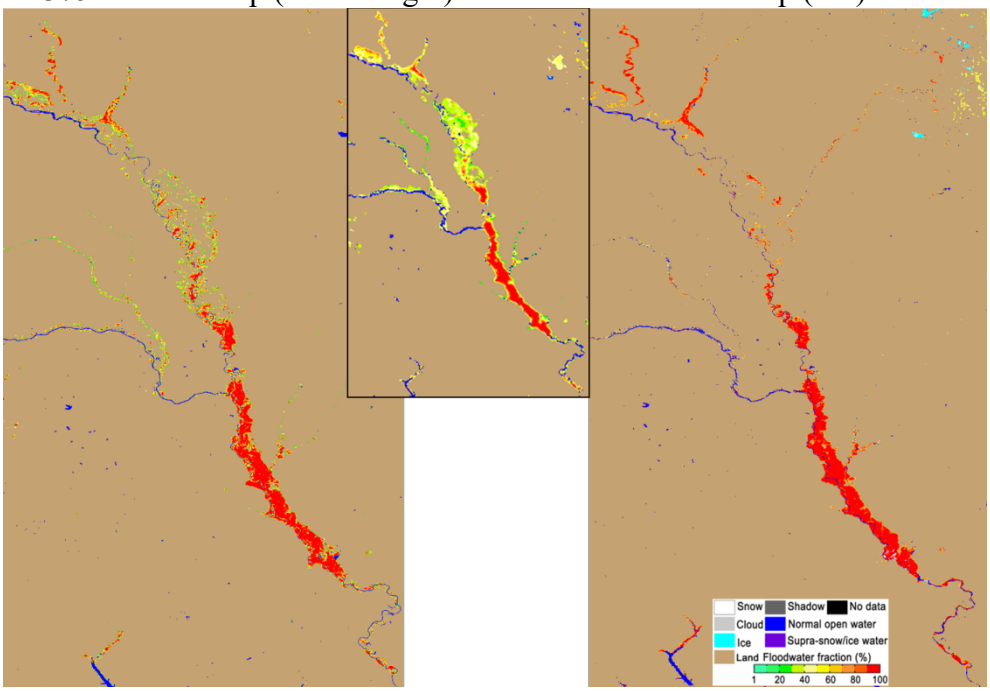

Fig. 2-7 ABI downscaled 375-m flood map (left) comparing with ABI 1-km flood map

(mid) and VIIRS 375-m flood map (right) on Mar. 21, 2019 along the Missouri River

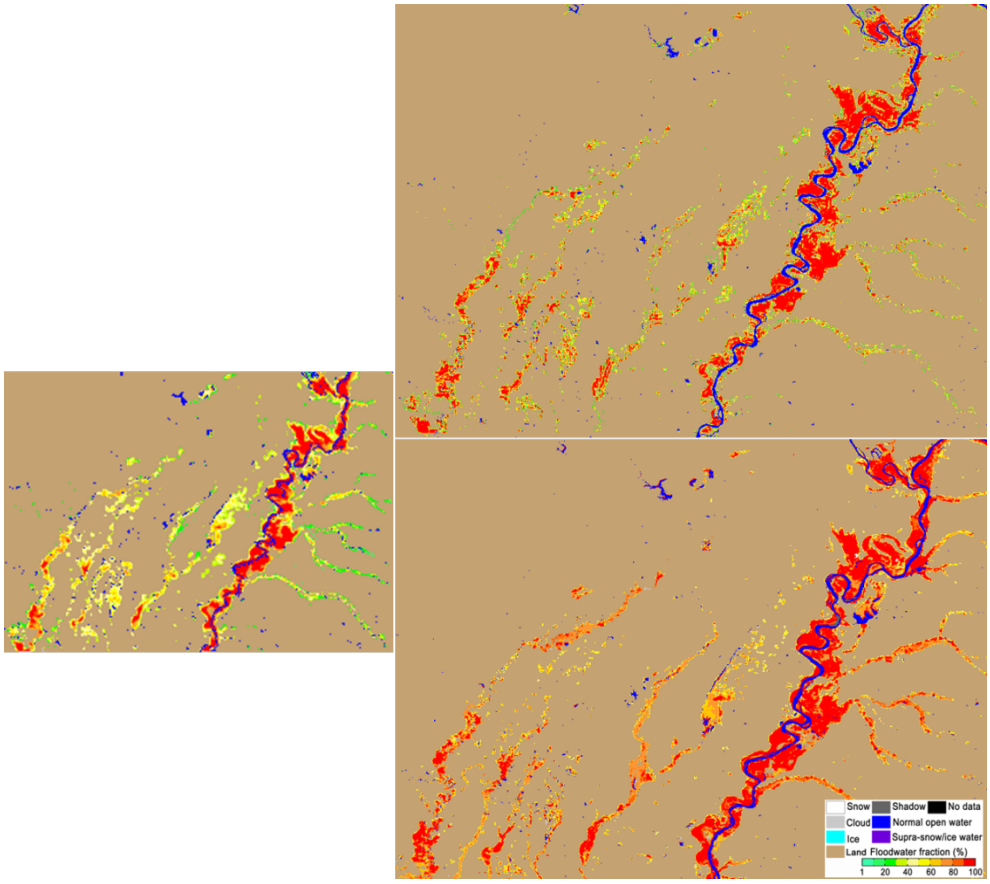

Fig. 2-8 ABI downscaled 375-m flood map (top right) comparing with ABI 1-km flood map (left) and VIIRS 375-m flood map (bottom right) on Mar. 16, 2019 along the Mississippi River

2.7.2 Quantitative comparison

The ABI downscaled 375-m flood maps are also compared with original ABI 1-km flood maps and VIIRS 375-m flood maps in a quantitative way. Number of pixels that are typed as flood in ABI flood maps but are detected as dryland in VIIRS flood maps ($\mathbf{N_1}$), number of pixels that are typed as dryland in ABI flood maps but are detected as flood in VIIRS flood maps ($\mathbf{N_2}$), and the total flood pixels in ABI and VIIRS flood maps ($\mathbf{N_t}$) are estimated. The absolute average water-fraction difference between ABI and VIIRS ($|\mathbf{D\_WF}|$) is calculated to compare the change of water fraction from the downscaling process. Based on $\mathbf{N_1}$, $\mathbf{N_2}$ and $\mathbf{N_t}$, two percentages $\mathbf{P_1}$ which is defined as $\frac{N1}{Nt} \times 100\%$ and $\mathbf{P_2}$ which is defined as $\frac{N2}{Nt} \times 100\%$ are also calculated.

Table 2-4 lists the quantitative comparison results against VIIRS flood maps between ABI downscaled 375-m flood maps and original ABI 1-km flood maps. In Table 2-4, altogether five regions are chosen for the comparison, which includes the 2017's Texas flood from hurricane Harvey, the 2019's Missouri River flood, the 2019's Mississippi river flood and the 2023's Red river flood.

From Table 2-4, the ABI downscaled 375-m flood maps have much improved results than the original ABI 1-km flood maps. The absolute average water-fraction difference between ABI and VIIRS is decreased, which means the downscaled ABI 375-m flood maps have much closer water fractions with VIIRS results. This is reasonable because the ABI downscaled flood maps have much better spatial resolution than the original ABI flood maps. The two percentages, which reflect water detection accuracy, also show improved quality from the downscaled ABI flood maps comparing to the ABI 1-km flood maps. Flood pixels in 1-km ABI flood maps are decreased 5% to 25% in the downscaled ABI flood maps due to the resolution enhancement.

Table 2-4 Quantitative comparison against VIIRS flood maps between ABI downscaled 375-m flood maps and original ABI 1-km flood maps

Region	**Resolution**	N_1	N_2	|D_WF|	N_t	P_1(%)	P_2(%)
1	ABI_1km	7297	16461	11	82938	9	20
	ABI_375m	4543	17783	10	82938	5	21
2	ABI_1km	18983	8769	20	75559	25	12
	ABI_375m	10419	10723	14	75559	14	14
3	ABI_1km	21137	2112	24	49842	42	4
	ABI_375m	10888	2848	20	49842	22	6
4	ABI_1km	6379	299	18	22014	29	1
	ABI_375m	3258	310	14	22014	15	1
5	ABI_1km	12201	7536	34	23721	51	32
	ABI_375m	3375	1258	12	23721	14	5

From the validation results, the ABI downscaled 375-m flood product is more consistent to the VIIRS flood product than the original ABI 1-km flood product. That means the blended VIIRS/ABI flood product with the simplified downscaling method is with better quality than that with the nearest neighboring interpolation method, and thus is used as the major flood detection dataset of the blended VIIRS/ABI flood product.

3 ASSUMPTIONS AND LIMITATIONS

The blended VIIRS/ABI flood product is based on the VIIRS and ABI daily composited flood product. It inherits the uncertainties from VFM and AFM products, and thus it inherits the assumptions and limitations from the two products. In addition, it has its own assumptions and limitations from the downscaling process.

The downscaling process assumes in each water polygon, water level is the same everywhere. However, when clustering floodwater pixels to water polygons, some floodwater pixels that have different water level may be counted in, which brings about uncertainties to the polygon water level estimation, and further affect the results from the downscaling process.

The downscaling process is a simplified process and does not consider the impact from tree cover and urban constructions. The polygon water levels are not corrected with river network analysis and dryland pixels around, which may decrease the accuracy of the downscaled results.

Other limitations are from CDSM data, which measures elevations of treetops, instead of bare ground. These may pose some impact on the downscaled results especially over regions with tree cover or urban constructions.

3.1 Performance Assumptions

The blended VIIRS/ABI flood product inherits the assumptions and limitations from ABI and VIIRS daily composited flood products. Unless the two products become available, the product is not processed.

The product is with the same geographic coverage with ABI flood product. It is based on VIIRS AOIs, and uses ABI clear-sky coverage to fill the gaps of cloud and cloud shadows in the VFM product. Only VIIRS AOIs from 11 to 41 are intersected with ABI flood maps, and if one AOI is fully coverage with ocean, it is not produced.

3.2 Potential Improvements

In future, the simplified downscaling process could be replaced with the full downscaling process by considering all the impact factors such as tree cover, urban constructions and so on.

Once the VIIRS and ABI downscaled 30-m floodwater depth product become available, the blended VIIRS/ABI flood product could be directly blended with the 30-m VIIRS/ABI floodwater depth products and becomes a blended VIIRS/ABI downscaled 30-m floodwater depth product.

4 REFERENCES

[1]. Ali, A., 1989.Study of river flood hydrology in Bangladesh with AVHRR data, Int.J. Remote Sens., vol. 10, pp. 1873–1892

[2]. Andrimont, R. D ,Bartholomé, E.&Defourny, P. (2012). 8 years water bodies monitoring analysis using MODIS over the Africancontinent. EGU General Assembly 2012, 12905

[3]. Barton, I. J.&Bathols,J. M. (1989).Monitoring floods with AVHRR,Remote Sensing of Environment, vol.30, no. 89–94

[4]. Brakenridge, G. R., Knox, J. C., Paylor, E. D., &Magilligan, F. J. (1994). Radar remote sensing aids study of the great flood of 1993,EOS Trans., AGU, 75(45), 521±527.

[5]. Brakenridge, G.R. & Anderson, E. (2006).MODIS-based Flood Detection, Mapping and Measurement: the Potential for Operational Hydrological Applications, Earth and Environmental Sciences, 72,1-12

[6]. Brakenridge, G R.(2011).Technical Description, DFO-GSFC Surface Water Mapping Algorithm,http://floodobservatory.colorado.edu/Tech.html

[7]. Brakenridge, G. R., Knox, J. C., Paylor, E. D., &Magilligan, F. J. (1994). Radar remote sensing aids study of the great flood of 1993, EOS Trans., AGU, 75(45), 521±527.

[8]. Carroll, M., Townshend, J.,DiMiceli, C.,Noojipady, P. &Sohlberg, R. (2009).A New Global Raster Water Mask at 250 Meter Resolution:, International Journal of Digital Earth, 2, 4

[9]. Ceccato, P., Flasse, S., and Gregoire, J.M.(2002). Designing a spectral index to estimate vegetation water content from remote sensing data: Part 2. Validation and applications. Remote Sensing of Environment 82: 198-207.
[10]. Croitoru, A., Crooks, A., Radzikowski, J., & Stefanidis, A. (2013). GeoSocial Gauge: A System Prototype for Knowledge Discovery from Social Media, International Journal of Geographical Information Science, 27(12): 2483-2508.
[11]. Cox, C.; Munk, W (1954). Statistics of the Sea Surface Derived from Sun Glitter. J. Mar. Res., 13, 198-227
[12]. Fisher, Adrian; Flood, Neil; Danaher, Tim (2016).Comparing Landsat water index methods for automated water classification in eastern Australia. Remote Sensing of Environment,Vol. 175,167-182
[13]. Gao, B. C. (1996). NDWI—A normalized difference water index for remote sensing of vegetation liquid water from space, Remote Sensing of Environment, 58:257-266 (1996)
[14]. Gumley, L.E. & King, M.D. (1995). Remote Sensing of Flooding in the U.S. Upper Midwest during the Summer of 1993, Bulletin of American Meteorological Society, 76, 6
[15]. Gupta, R. P. & Banerji, S. 1985. `Monitoring of reservoir volume using Landsat data', J. Hydrol., 77, 159±170.
[16]. Gupta, R. P. &Bodechtel, J. 1982. `Geotechnical applications of Landsat image analysis of Bhakra dam reservoir, India', RemoteSens. Environ., 12, 3±13.
[17]. Hutchison, K. D., Mahoney, R. L., Vermonte, E. F., Kopp, T. J., Jackson, J. M., Sei, A., and Iisager, B. D.(2009). A Geometry-Based Approach to Identifying Cloud Shadows in the VIIRS Cloud MaskAlgorithm for NPOESS, Journal of Atmospheric and Oceanic Technology 26: 1388–1397.
[18]. International Federation of the Red Cross and Red Crescent Societies (IFRC). *World Disasters Report*; Oxford University Press: Oxford, UK, 2008; ISBN 978-92-9139-156-1.
[19]. Jin, Y. Q. (1999). Flooding index and its regional threshold value for monitoring floods in China from SSM/I data. International Journal of Remote Sensing, 20(5): 1025-1030.
[20]. Johansson, A. M.& Brown, I. A. (2013). Adaptive classification of supraglacial lakes on the West Greenland ice sheet. IEEE Journal of Select Topics Appl. Earth Obs. Remote. Sens., 6(4), 1998-2007 (doi: 10.1109/JSTARS.2012.2233722)
[21]. Khlopenkov, K. V. and Trishchenko, A. P. (2007). New cloud, snow, and cloudshadow detection scheme for historical 1-km AVHHR data over Canada.*J. Atmos. Oceanic Tech.*, vol. 24, pp. 322−343.
[22]. Kundzewicz, Z.W.; Schellnhuber, H.J. (2004). Floods in the IPCC TAR perspective. *Nat. Hazards*, *31*, 111–128.
[23]. Lesson, A. A. Leeson, Shepherd, A., Sundal, A. V., Johansson, A. M., Selmes, N., Briggs, K., Hogg, A. E. &Fettweis, X. (2013). A comparison of supraglacial lake observations derived from MODIS imagery at the western margin of the Greenland ice sheet, Journal of Glaciology, Vol. 59, No. 218
[24]. Liang, Y.-L., Colgan, W., Lv, Q., Steffen, K., Abdalati, W., Stroeve, J., Gallaherb, D., Bayou, N. (2012). A decadal investigation of supraglacial lakes in

West Greenland using a fully automatic detection and tracking algorithm, Remote Sensing of Environment, Volume 123, August 2012, Pages 127–138
[25]. Li, S., Sun, D.L., Goldberg, M. D , Kalluri, S., Sjoberg, B., Lindsey, D., Hoffman, J.P., DeWeese, M., Connelly, B., Mckee, P. and Lander, K. (2022). A downscaling model for derivation of 3-D flood products from VIIRS imagery and SRTM/DE, ISPRS Journal of Photogrammetry and Remote Sensing, 192 (2022) 279–298
[26]. Li, S. & Sun, D.(2013). Development of an integrated high resolution flood product with multi-source data, UMI Dissertations Publishing 2013, ISBN: 9781303635939, http://search.proquest.com/docview/1492669000, 2013
[27]. Li, S., Sun, D.L. & Yu,Y.Y. (2013). Automatic cloud-shadow removal from flood/standing water maps using MSG/SEVIRI imagery, International Journal of Remote Sensing, 34:15, 5487-5502
[28]. Li, S., Sun, D.L., Goldberg, M. D. &Sjoberg, B. (2015). Object-based Automatic Terrain Shadow Removal from SNPP/VIIRS Flood Maps, International Journal of Remote Sensing, Vol. 36, No. 21, 5504–5522
[29]. Li, S., Sun, D. L.,Yu, Y. Y.,Csiszar, I.,Stefanidis, A. & Goldberg, M. D. (2012).A New Shortwave Infrared (SWIR) Method for Quantitative Water Fraction Derivation and Evaluation with EOS/MODIS and Landsat/TM data, IEEE Transactions on Geoscience and Remote Sensing,99
[30]. Li, S., Sun, D.L., Goldberg, M. D&Stefanidis, A. (2013).Derivation of 30-m-resolution Water Maps from TERRA/MODIS and SRTM, Remote Sensing of Environment 134 (2013) 417–430
[31]. Liu, Yan Y,.Maidment, D. R., Tarboton, D. G., Zheng, X., Yildirim, A., Sazib, N. S., Wang, S. W. (2016). “A CyberGIS Approach to Generating High-resolution Height Above Nearest Drainage(HAND) Raster for National Flood Mapping.” CyberGISCenter Technical Report (2016).
[32]. Martinis, S., Twele, A., Strobl, C., Kersten, J., and Stein, E. (2013).A Multi-Scale Flood Monitoring System Based on Fully Automatic MODIS and TerraSAR-X Processing Chains. Remote Sensing, 5:5598-5619.
[33]. Martinis, S., Twele, A., and Voigt, S. (2009) Towards operational near real-time flood detection using a split-based automatic thresholding procedure on high resolution TerraSAR-X data, Nat. Hazards Earth Syst. Sci., 9, 303-314, doi:10.5194/nhess-9-303-2009.
[34]. Matgen, P., Schumanna, G., Henryc, J.-B., Hoffmanna, L. &Pfistera, L. (2007). Integration of SAR-derived river inundation areas, high-precision topographic data and a river flow model toward near real-time flood management.International Journal of Applied Earth Observation and Geoinformation, 9, 247-263
[35]. Matgen, P., Hostache, R., Schumann, G., Pfister, L., Hoffmann, L., and Savenije, H. (2011). Towards an automated SAR-based flood monitoring system: lessons learned from two case studies. Physics and Chemistry of the Earth, 36:241-252.
[36]. Montagner F, Billat V, Bélanger S (2003) MERIS ATBD 2.13 - Sun glint flag algorithm, issue 4,revision 2
[37]. Mueller, N., Lewis, A., Roberts, D., Ring, S., Melrose, R., Sixsmith, J., Lym-Burner, L., McIntyre, A., Tan, P., Curnow, S., and Ip, A. (2016). Water observations from space: Mapping surface water from 25 years of Landsat imagery across Australia. Remote Sensing of Environment, 174:341-352.

[38]. Pulvirenti, L., Pierdicca, N., Chini, M., and Guerriero, L. (2011) An algorithm for operational flood mapping from Synthetic Aperture Radar (SAR) data using fuzzy logic, Nat. Hazards Earth Syst. Sci., 11, 529-540, doi:10.5194/nhess-11-529-2011.
[39]. Rabus, B., Eineder, M., Roth, A. andBamler, R.(2003). The shuttle radar topography mission- a new class of digital elevation models acquired by spaceborne radar, Photogramm. Rem. Sens., v. 57, p. 241-262.
[40]. Rouse, J.W, Haas, R.H., Scheel, J.A., and Deering, D.W. (1974). Monitoring Vegetation Systems in the Great Plains with ERTS,Proceedings, 3rd Earth Resource Technology Satellite (ERTS) Symposium, vol. 1, p. 48-62.
[41]. Schumann, G.,Hostache, R.,Puech,C.,Hoffmann,L.,Matgen,P., Pappenberger, F.&Pfister, L. (2007).High-Resolution 3-D Flood Information From Radar Imagery for Flood Hazard Management. IEEE Transactions on Geoscience and Remote Sensing, 45, 1715-1725.
[42]. Schroeder, W., Prins, E., Giglio, L., Csiszar,I., Schmidt, C.,Morisette, J., Morton, D.(2008).Validation of GOES and MODIS active fire detection products using ASTER and ETM+ data, Remote Sensing of Environment, 112 (2008) 2711–2726
[43]. Sellers, P. J. (1985).Canopy reflectance, photosynthesis, and transpiration, International Journal of Remote Sensing, 6, 1335-1372
[44]. Sheng, Y. & Xiao, Q. (1994). Water Identification in Cloud-contaminated NOAA/AVHRRImagery, Remote Sensing of Environment in China, vol. 9, pp. 247–255
[45]. Sheng, Y., Su,Y. & Xiao, Q. (1998). Challenging the cloud-contamination problem in floodmonitoring with NOAA/AVHRR imagery, Photogrammetric Engineering RemoteSens., 64, 191–198
[46]. Sheng, Y. & Gong, P. (2001). Quantitative dynamic flood monitoring with NOAA AVHRR, Int. J. Remote Sens., vol. 22, no. 9, pp. 1709–1724
[47]. Shepard, M. K., Campbell, B. A., Bulmer,M. H., Farr,T. G., Gaddis, L. R. and Plaut, J. J.(2001). The roughness of natural terrain: A planetary and remote sensing perspective, Journal of Geophysical Research, Vol. 106, NO. El2, Pages 32,777-32,795
[48]. Sippel, S. J., Hamilton, S. K., Melack, J. M., and Choudhury, B. J. (1994). Determination of inundation area in the Amazon river floodplain using the SMMR 37 GHz polarization difference. Remote Sensing of Environment, 48 (1), 70–76.
[49]. Stefanidis, A., Crooks, A., & Radzikowski, J. (2013). Harvesting Ambient Geospatial Information from Social Media Feeds, Geojournal, 78(2): 319-338.
[50]. Sun, D. L., Yu, Y. Y., Zhang, R., Li, S. &Goldberg, M. D. (2012).Towards Operational Automatic Flood Detection Using EOS/MODIS data, Photogrammetric Engineering & Remote Sensing, 78 (6), 637-646
[51]. Tachikawa, T., Hato, M., Kaku, M. and Iwasaki, A.(2011). The characteristics of ASTER GDEM version 2, IGARSS, July 2011
[52]. Tanaka, M., Sugimura, T., Tanaka, S., and Tamai, N. (2003). Flood drought cycle of Tonle Sap and Mekong Delta area observed by DMSP-SSM/I. International Journal of Remote Sensing, 24 (7), 1487–1504.
[53]. Thompson, R. J., Oosterom, P.V.,Zlatanova,S.,Giesen, N. V. D. and Goulevitch,B. (2011). Monitoring the Extent of Flooding – Based on a Case Study in

Queensland, the International Archives of the Photogrammetry, Remote Sensing and Spatial Information Sciences, Vol. 34, Part XXX
[54]. Ticehurst, C., Guerschman, J.P., Chen, Y. (2014). The strengths and limitations in using the daily MODIS open water likelihood algorithm for identifying flood events. Remote Sensing 6 (12), 11791-11809
[55]. Ticehurst, C., Dutta, D., Karim, F., Petheram, C., Guerschman, J.P. (2015). Improving the accuracy of daily MODIS OWL flood inundation mapping using hydrodynamic modelling. Natural Hazards 78 (2), 803-820
[56]. Tsugawa, R. and James, B (2011). Joint Polar Satellite System (JPSS) VIIRS Snow Cover Algorithm Theoretical Basis Document, NPOESS Common Data Format Control Book – External Volume 5 Metadata,D34862-05
[57]. Tulbure, Mirela G.; Broich, Mark; Stehman, Stephen V.; et al. (2016) Surface water extent dynamics from three decades of seasonally continuous Landsat time series at subcontinental scale in a semi-arid region. Remote Sensing of Environment, Vol.178,142-157
[58]. Wang,Y.,Colby,J. D. &Mulcahy, K. A.(2002). An efficient method for mapping flood extent in a coastal floodplain using Landsat TM and DEM data. International Journal of Remote Sensing, 23:18, 3681-3696
[59]. Wiesnet, D.R., McGinnis,D.V. & Pritchard, J.A. (1974). Mapping of the 1973 Mississippi river floods by the NOAA-2 Satellite, Water Resources Bulletin, 10(5), 1040-1049
[60]. Xian, G., Homer, C., and Fry, J., (2009). Updating the 2001 National Land Cover Database land cover classification to 2006 by using Landsat imagery change detection methods. Remote Sensing of Environment, 113, 1133-1147
[61]. Xiao, X.G., Shen, Z.X.,and Qin, X. G. (2001). Assessing the potential of VEGETATION sensor data for mapping snow and ice cover: a Normalized Difference Snow and Ice Index, International Journal of remote sensing, 2001, vol. 22, no. 13, 2479–2487
[62]. Weng, F., Yang, H., and Zou, X. (2013). On Convertibility from antenna to sensor brightness temperature for ATMS. IEEE Geophysical Research Letters, 10 (4), 771-775.
[63]. Zhang Y. X., Zhang L.J., Huang Y. F., Rong, Z. G., Hu, X. Q., Liu, J.J. and Zhang, G. S. (2008). Spectral Data Sets for Satellite Calibration Site and Typical Earth Objects, M., China Meteorological Press, ISBN: 978-7-5029-4422-3
[64]. Zheng, W., Liu, C., Wang, Z. X, and Xin, Z. B. (2008). Flood and waterlogging monitoring over Huaihe River Basin by AMSR-E data analysis. China Geographic Science, 18 (3), 262-267.